Application of the Peridynamic Theory in the Stress Field Analysis of Plates with Geometric Discontinuities

Átila Lupim Cruz [1], Maurício Vicente Donadon [2]

[1] Mechanical Division, Institute of Aeronautics and Space-IAE, Praça Marechal Eduardo Gomes, 50, Vila das Acácias, 12228-904, São José dos Campos, São Paulo, Brazil

[2] Aeronautical Engineering Division-IEA-E, Technological Institute of Aeronautics-ITA, Praça Marechal Eduardo Gomes, 50, Vila das Acácias, 12228-900, São José dos Campos, São Paulo, Brazil

Abstract: One of the methods developed in recent years for the numerical solution of elastodynamics problems is the Peridynamic Theory. This method has, among others advantages, a natural capacity to simulate the initiation and growth of cracks in solid materials without the aid of additional methods and/or numerical procedures commonly employed in the conventional finite element formulation. This is mainly because the formulation behind the peridynamic theory is not based on partial derivatives of displacement fields, but based on the partial integrals of this field. Within this context, this paper presents a numerical investigation on the accuracy of the peridynamic theory to predict the stress and strain fields in isotropic plates with different geometric discontinuities, when subjected to different loading and boundary conditions in the elastic and plastic regimes. These results are compared with analytical solutions and numerical results showed in literature, and conclusions will be drawn.

Keywords: Peridynamic, plates with discontinuities, stress analysis

INTRODUCTION

One of the methods developed in recent years for the numerical solution of elastodynamics problems is the Peridynamic Theory. This method has, among other advantages, a natural capacity to simulate the initiation and growth of cracks in solid materials, without the need of additional methods and numerical procedures commonly used in finite element formulations (Sarego et al., 2016).

This advantage is due to the constitutive relations of peridynamics not being formulated using partial derivatives of the displacement field, but rather based on partial integrals of this field. With the appearance of a crack or other kind discontinuity, the peridynamics constitutive equations continue to be definite (Bobaru et al., 2017).

The peridynamics theory is a meshless method. Thus, in a numerical simulation, a cloud of points represents the domain, where each point represents a small volume of material. In this theory, each point interacts with the others by prescribed response functions, which contains all the constitutive information associated with the simulated material. These interactions can only occur between points that are within a maximum distance, defined as the horizon (Bobaru et al., 2017).

A very small value for horizon can influence the crack growth by discretization orientation. On the other hand, a large value can cause an excessive wave dispersion within the simulated domain, and increase the computational cost without a good gain in accuracy (Bobaru et al., 2017).

For simulations involving deformations in the plastic regime, a constitutive relation for peridynamic theory based on the Von Mises flow criterion with isotropic hardening was developed. In the literature, these elastoplastic relationships have a good accuracy in the simulation of plastic isotropic plates, including simulating residual plastic deformations after an unloading process (Madenci and Oterkus, 2016).

The peridynamic theory calculates the displacement field of a given domain. With this, the computation of stress and strain fields cannot be obtained natively in this method. Thus, from these displacements, the strains are calculated and, through constitutive relations of solid mechanics, the stresses obtained. For elastoplastic analyzes, it is verified if the stress field exceeds the yield surface defined by the constitutive relations of peridynamics. If necessary, a method based on Von Mises flow criterion can be used to correct the stresses (Villani et al., 2015).

BASIC THEORY

The peridynamic state-based equation of motion used in this paper is presented in Madenci and Oterkus (2014) and Madenci and Oterkus (2016). This equation is also showed below, where ρ is the material density, b is the vector of external loads, V is the volume of a material point and N is the number of points inside the horizon of a point k in the simulated domain.

$$\rho_{(k)}\ddot{u}_{(k)} = \sum_{j=1}^{N}\left[t_{(k)(j)}\left(u_{(j)}-u_{(k)}, x_{(j)}-x_{(k)}, t\right) - t_{(j)(k)}\left(u_{(k)}-u_{(j)}, x_{(k)}-x_{(j)}, t\right)\right]V_{(j)} + b_{(k)} \tag{1}$$

The force density vector $t_{(k)(j)}$ is defined by:

$$t_{(k)(j)} = \left[\left(a_k - a_\mu\right)2\delta d\frac{\Lambda_{(k)(j)}}{\left|x_{(j)}-x_{(k)}\right|}\theta^e_{(k)} + 2\delta b s^e_{(k)(j)}\right]\frac{y_{(j)}-y_{(k)}}{\left|y_{(j)}-y_{(k)}\right|} \tag{2}$$

Where the dilatation $\theta_{(k)}$, stretch $s_{(k)(j)}$ and $\Lambda_{(k)(j)}$ are:

$$\begin{aligned}
&\theta^e_{(k)} = d\delta\sum_{j=1}^{N} s^e_{(k)(j)}\Lambda_{(k)(j)}V_{(j)} \;\;;\;\; s^e_{(k)(j)} = \frac{\left|y_{(j)}-y_{(k)}\right| - \left|x_{(j)}-x_{(k)}\right|}{\left|x_{(j)}-x_{(k)}\right|} - s^{pl}_{(k)(j)} \\
&\Lambda_{(k)(j)} = \frac{y_{(j)}-y_{(k)}}{\left|y_{(j)}-y_{(k)}\right|}\frac{x_{(j)}-x_{(k)}}{\left|x_{(j)}-x_{(k)}\right|}
\end{aligned} \tag{3}$$

The constants a_k, a_μ, b and d, for a 2D analysis, are defined in Madenci and Oterkus (2014) as:

$$a_k = \frac{k}{2} \;\;;\;\; a_\mu = \mu \;\;;\;\; b = \frac{6\mu}{\pi h\delta^4} \;\;;\;\; d = \frac{2}{\pi h\delta^3} \tag{4}$$

In which k is the bulk modulus, μ is the shear modulus, h is the thickness of the simulated domain, δ is the horizon defined for the simulation, x is the coordinate in non-deformed space and y is the coordinate in the deformed space. For this paper, the horizon is defined as 3 times greater than the distance between points, as recommended by Bobaru et al. (2017).

The term $s^{pl}_{(k)(j)}$ is the plastic part of stretch. This value is obtained using the methodology described in Madenci and Oterkus (2016). The strain field is obtained by using a forward difference method between points inside the domain. The stress field is obtained by the elastoplastic methodology described in Villani et al. (2015) using the aforementioned strain field.

The time integration scheme used with this method is the adaptive dynamic relaxation method described in Oakley and Knight (1995). The stable time step is calculated by the Courant–Friedrichs–Lewy approach as presented in Bobaru et al. (2017).

This method is implemented in an in-house FORTRAN code, using all equations and definitions described here. In order to validate the code and verify the accuracy of the method, predicted results were compared with analytical solutions and numerical results reported in the open literature simulations for plates with and without geometric discontinuities.

PROBLEM FORMULATION

The accuracy checks are performed through five tests, where each test allows the evaluation of a part of the numerical program implemented for this research. The first test involves verifying the accuracy of a simulated plate under tensile loading in its elastic regime, and the predicted results compared with closed form solutions obtained from elasticity theory. The second test evaluates the shape of the stress strain curve for a plate under loading in the plastic regime, observing the accuracy of the plastic corrections. The third test is similar to the second one, but the imposed load is reduced during the simulation so that the slope of the elastic unload region could be verified. Finally, in the fourth and fifth tests, the plate has two kinds of geometric discontinuities to evaluate the concentration of stresses when loaded in the plastic regime: a central hole and a central crack, respectively.

In all tests the same plate is simulated, being defect-free for the first three tests, and with a central hole for the fourth test and a central crack for the fifth test, as show in the Figure 1. The physical properties of this plate are Poisson modulus 0.342, density 4428kg/m³, yield stress 1.017GPa, elastic modulus 113GPa and tangent modulus 1.38GPa. The

dimensions of the plate are height 1000mm, width 1000mm, diameter of hole 300mm and length of crack 300mm. In the first three tests, the additional dimensions of the plate are thickness 10mm, distance between points in discretization 10mm and thickness of the boundary layer 60mm. For the last two tests, the plate has thickness of 2.5mm, distance between points in discretization of 2.5mm and thickness of the boundary layer equals 15mm.

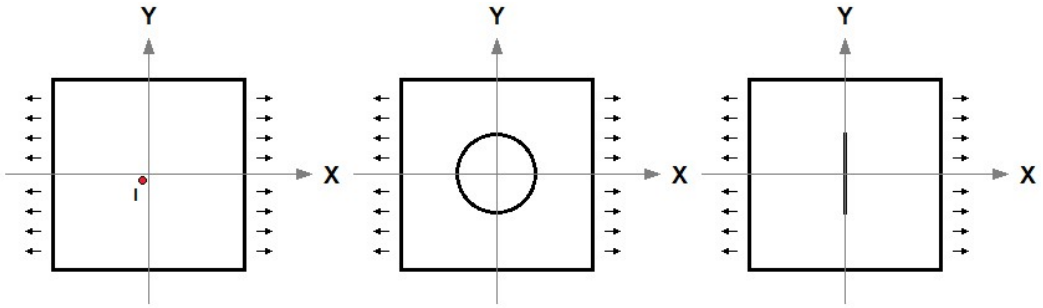

Figure 1 – The simulated plate for first to three tests (left), fourth test (center) and fifth test (right).

For the first test (T1), deformations of ε_x=5mm/m and ε_y=-$\nu\varepsilon_x$ are imposed on the indicated edges of the plate, which produces an equivalent deformation of ε_{eq}≈5.08mm/m. For the second (T2) and third tests (T3), the imposed deformations are ε_x=141mm/m and ε_y=-$\nu\varepsilon_x$, which results in an equivalent deformation of ε_{eq}≈143.33mm/m. In the third test, when the equivalent deformation reaches the value of 68mm/m, the load is reduced until reaching the value of 62.5mm/m. Immediately afterwards, the loading is increased to the final prescribed value. Finally, for the fourth (T4) and fifth tests (T5), a displacement is applied on the sides of the plate with a value of u_x=4mm and u_y=0mm. The loads are applied with a linear factor of 1/1000 at each step of time for the first test, 1/200000 for the second and the third tests, and 1/50000 for the fourth and fifth tests.

NUMERICAL RESULTS

First test (T1)

For the first test, the results of the equivalent stress and strain fields are shown below:

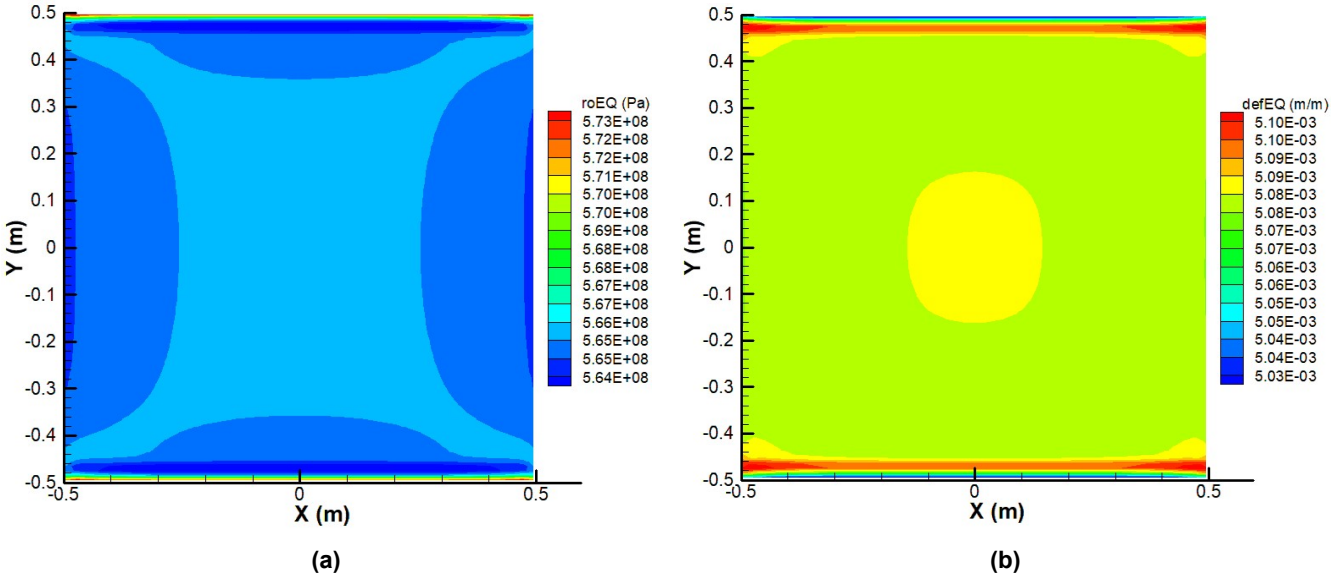

Figure 2 – (a) Equivalent stress field and (b) equivalent strain field for loading condition T1.

The result for the strain field is very close to those prescribed, even with the already known free surface error from peridynamics. The maximum error in the equivalent stress field is 1.5106%, while the average error in the domain for this same field is 0.0806%. For the equivalent strain field, the maximum error is 0.0053%, while the average error is 0.0003%.

Another way for obtaining the equivalent stress field is showed in Madenci and Oterkus (2016). The authors calculated this field using the distortional part of the strain energy density obtained by the peridynamic theory. This "peridynamic" equivalent stress field is shown below:

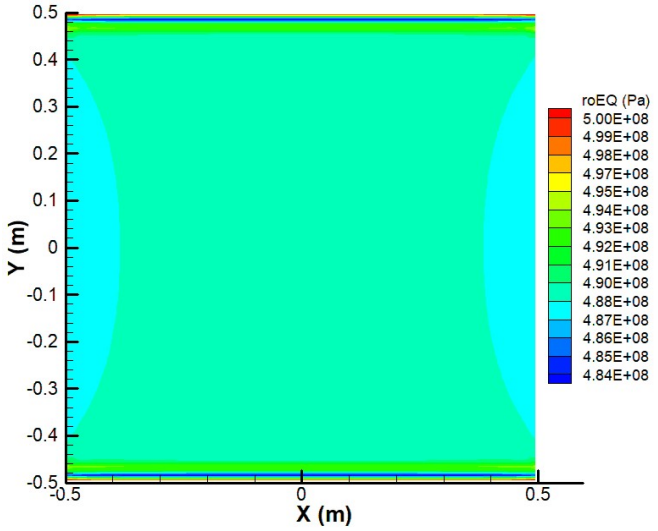

Figure 3 – Equivalent stress field obtained with peridynamic strain energy density for loading condition T1.

The accuracy for this stress field is much lower than that calculated by the classic elastic theory showed in Figure 2. The maximum error in the equivalent stress field is 14.6254%, while the average error in the domain for this same field is 13.4496%. The displacements fields for the first test are shown below:

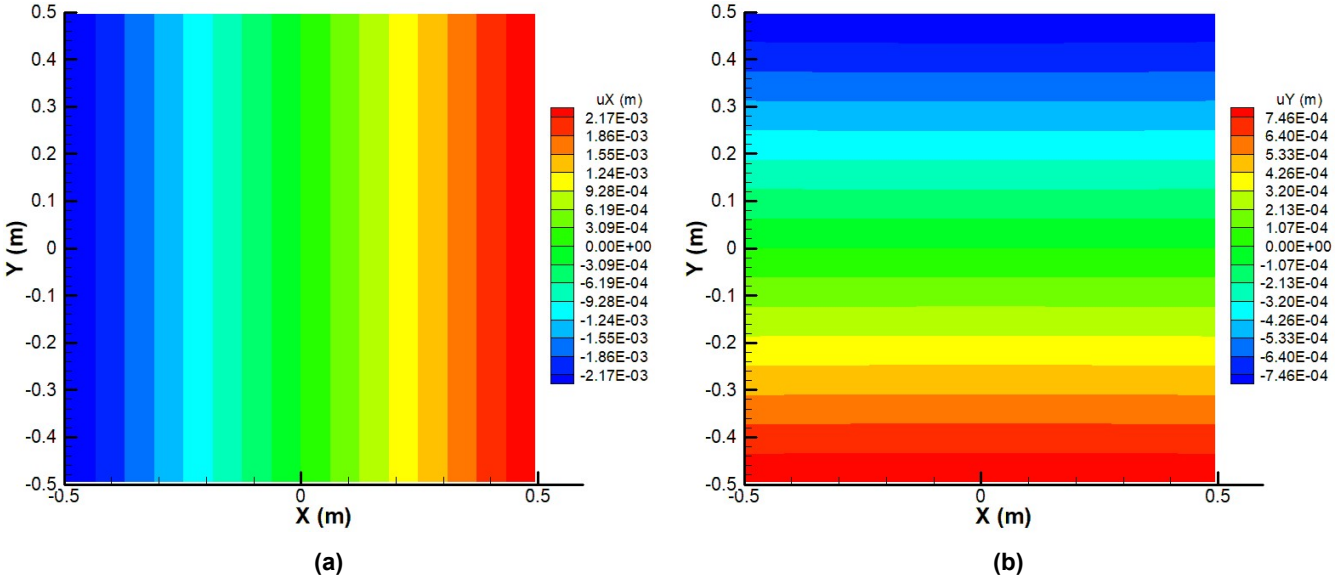

Figure 4 – (a) Displacement field on the X-axis and (b) displacement field on Y-axis for loading condition T1.

The results for the displacements fields are very close to the analytical ones. The maximum error in the displacements in the X-axis direction is 0.0557%, while the average error is 0.0245%. For the displacements in Y-axis direction, the maximum error is 0.0007%, while the average error is 0.0002%.

Analyzing the results, is noted the high accuracy returned by the implemented program for the stress, strain and displacements fields. Besides the excellent accuracy on the displacements, the stress field obtained by the peridynamic strain energy density resulted values very different from those expected.

Second and third tests (T2 and T3)

For the second and third tests, the equivalent stresses by equivalent strains for the point I (the most central point in the domain) are shown below:

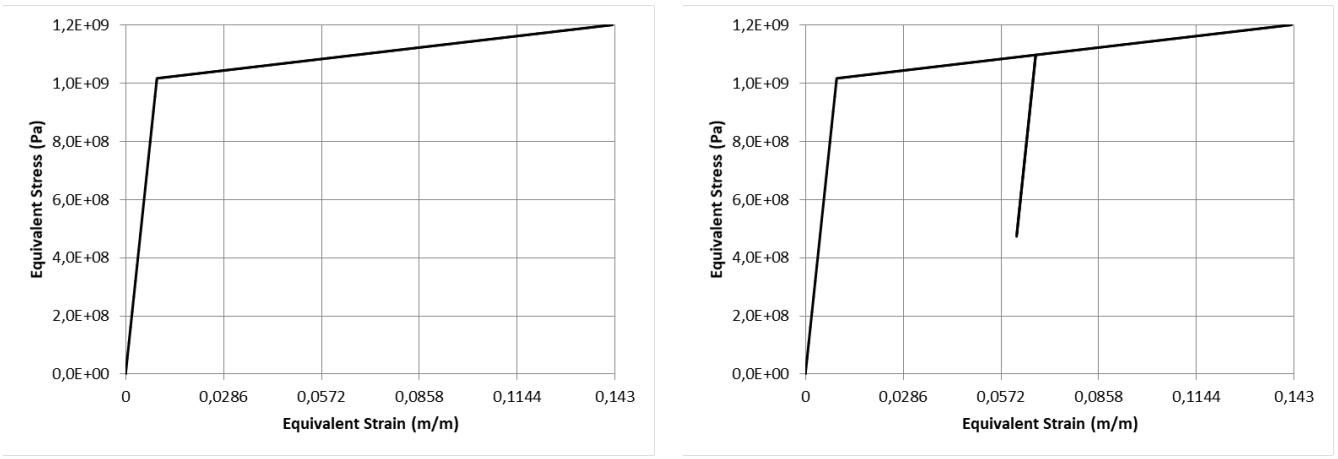

Figure 5 – Equivalent stress for different loading conditions: (a) T2 and (b) T3.

It should be noted that the results obtained are close to what is expected. The yield started in the predicted region and the simulation followed until the imposed final equivalent deformation. In addition, the unloading occurred as expected, with the slope compatible with the elastic region, and the yield resumed in the exact spot.

Fourth test (T4)

For the fourth test, the equivalent stress field and equivalent plastic stretch field are shown below:

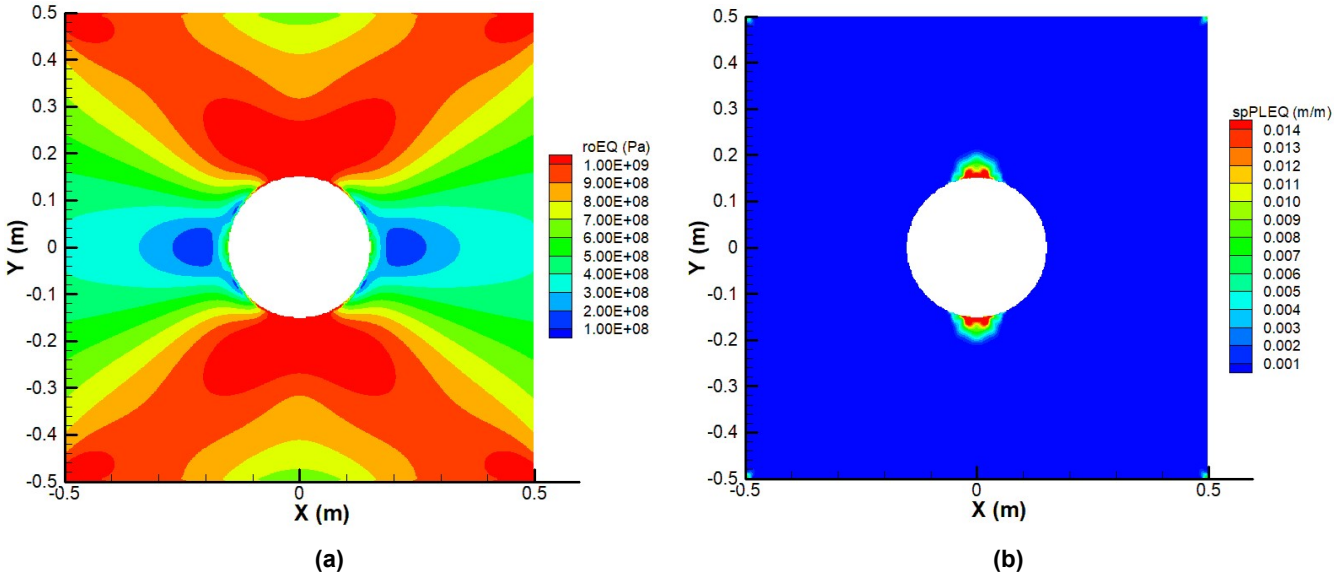

Figure 6 – (a) Equivalent stress field and (b) equivalent plastic stretch field for loading condition T4.

The effect of the stress concentration occurred in the region of the central hole, as expected. The displacement imposed on the plate, without the hole, would produce uniform stress and strain distributions in the elastic regime. With this concentration, the regions above and below the hole have a permanent plastic strain, which is also expected. For comparison, the results presented by Madenci and Oterkus (2016) for the same load condition are shown below:

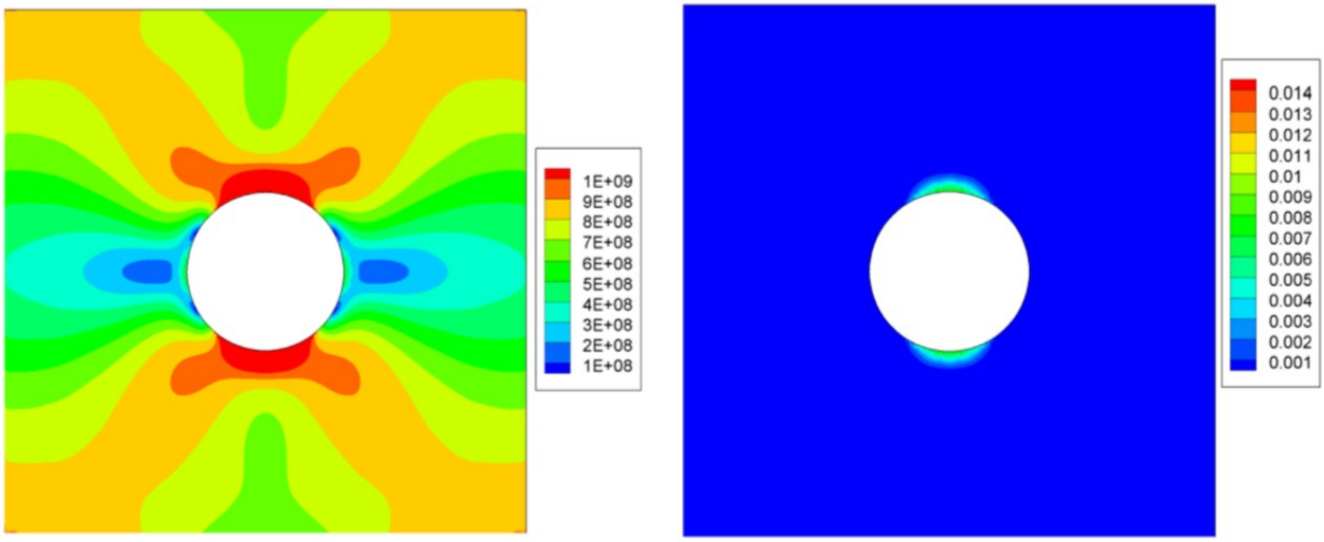

(a) **(b)**

Figure 7 – (a) Equivalent stress field and (b) equivalent plastic stretch field for loading condition T4 presented in Madenci and Oterkus (2016).

Analyzing the results found by the authors, is noted that the presented program returned values of stress higher than the ones reported in the literature. This discrepancy was observed in the first test presented in this paper (T1), where the equivalent stress field obtained by the authors was lower than those obtained by the classical approach. To verify this result, in Figure 8 is shown the results obtained by the authors using the same plate with a displacement of u_x=5mm and u_y=0mm (1mm higher than the load condition T4):

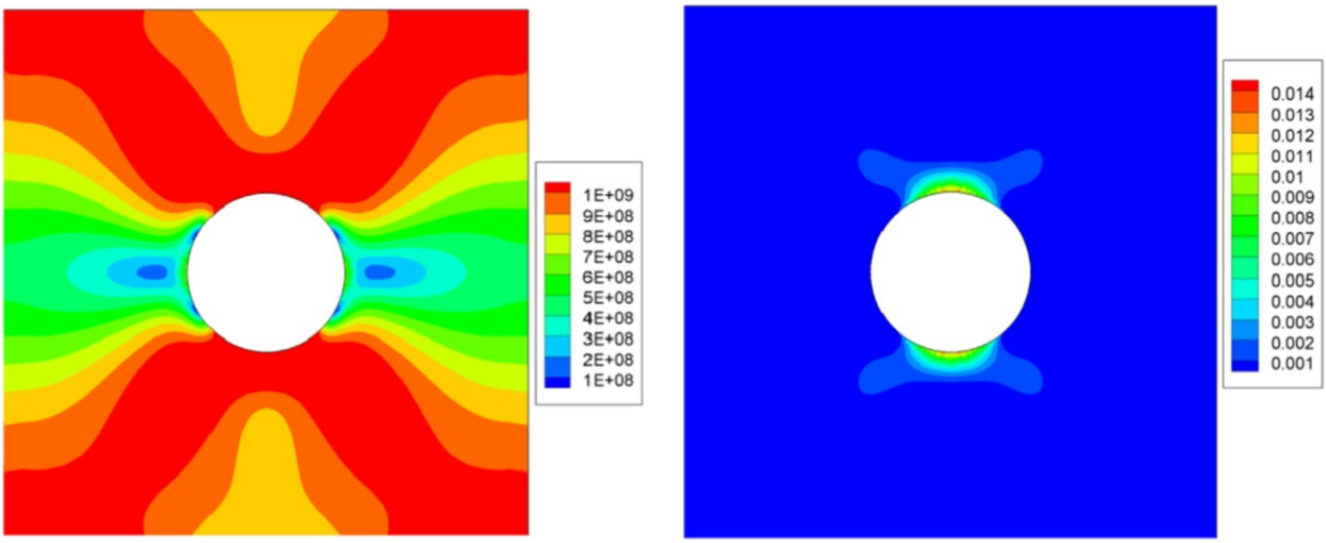

(a) **(b)**

Figure 8 – (a) Equivalent stress field and (b) equivalent plastic stretch field for u_x=5mm and u_y=0mm presented in Madenci and Oterkus (2016).

The shape of the stress field obtained by the numerical program is in between the two load conditions presented by the authors, which suggest the difference is caused by the same effect observed in the first test (T1).

Fifth test (T5)

Finally, for the fifth test, the equivalent stress field and equivalent plastic stretch field are shown below:

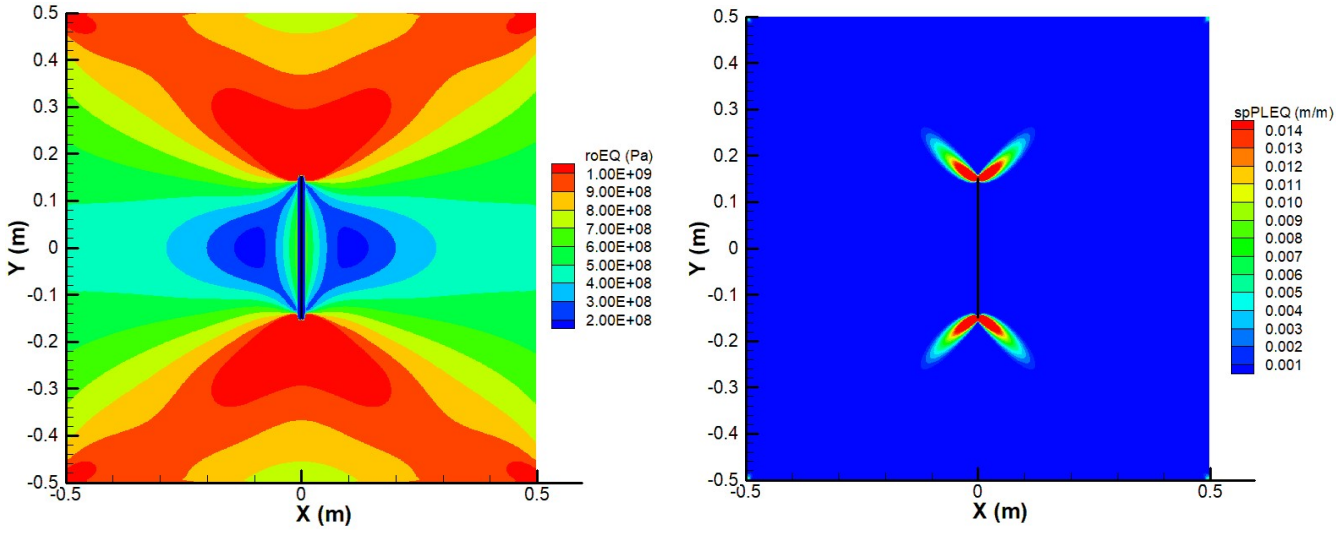

Figure 9 – (a) Equivalent stress field and (b) equivalent plastic stretch field for loading condition T5.

The effect of the stress concentration occurred in the region of the central crack, as expected. For comparison, the results presented by Madenci and Oterkus (2016) for the same load condition are shown below:

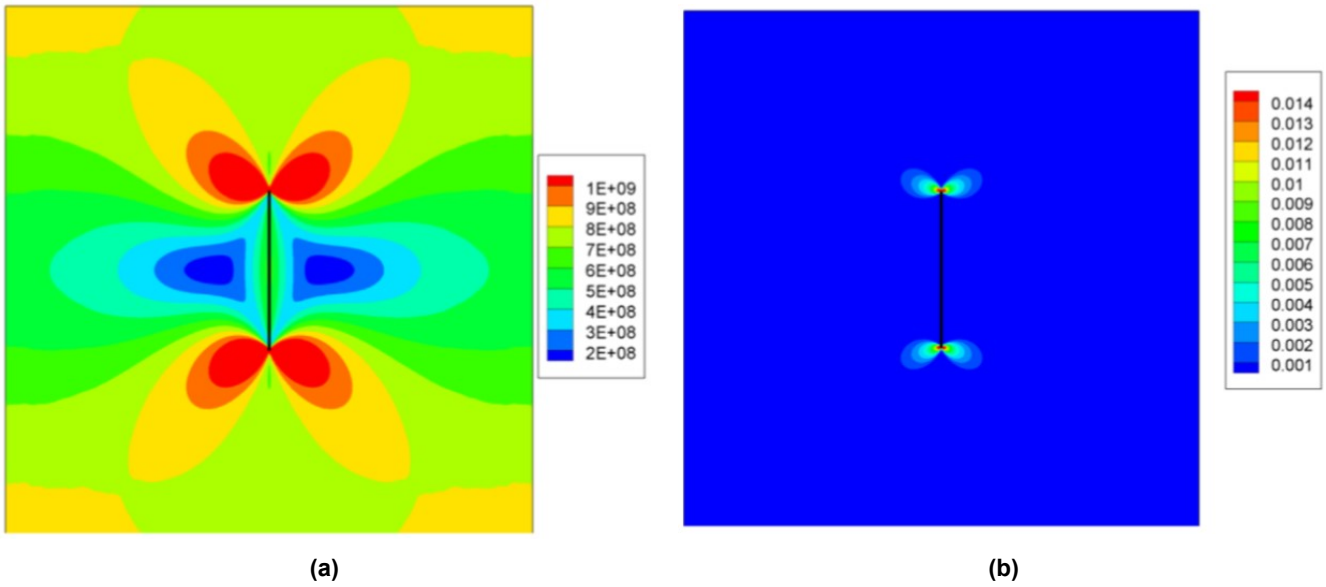

Figure 10 – (a) Equivalent stress field and (b) equivalent plastic stretch field for loading condition T5 presented in Madenci and Oterkus (2016).

The divergence in the numerical results has the same origin of the difference observed in the first and fourth tests. Like in the fourth test, the results obtained by the authors using the same plate with a displacement of u_x=5mm and u_y=0mm (1mm higher than the load condition T5) is shown below:

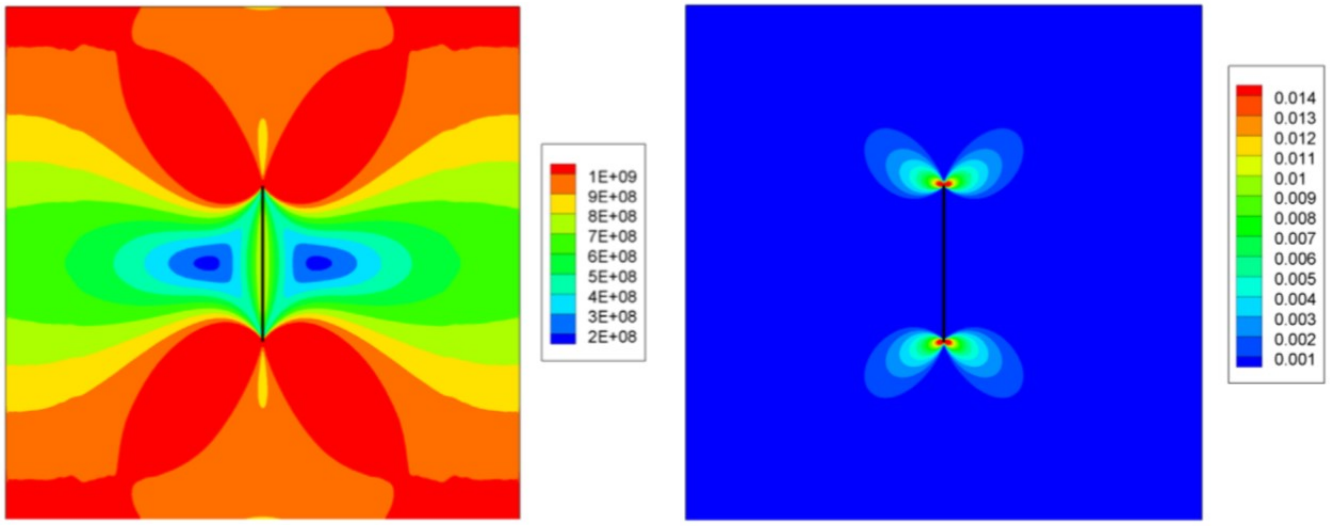

Figure 11 – (a) Equivalent stress field and (b) equivalent plastic stretch field for u_x=5mm and u_y=0mm presented in Madenci and Oterkus (2016).

CONCLUSIONS

This paper presented a peridynamic theory based formulation for stress analysis of plates in the elastic and plastic regimes. The formulation was implemented into an in-house FORTRAN based code. Some validation cases were presented and discussed. In general, good correlation between numerical predictions obtained using the proposed formulation and analytical and numerical results reported in the open literature was found. Some differences were observed in the equivalent stress fields obtained by the classical elastoplastic theory and by using the distortional strain energy density calculated by the peridynamic theory. The accuracy presented in the first test shows that the formulation has been correctly implemented, including the strain and stress fields calculation modules, which is not native to peridynamics.

The second and third tests show that the plasticity correction is working correctly and the unloading of the third test returns the same curve as the elastic regime. In addition, the stress concentration of the fourth and fifth tests occurred at the expect locations, and with the appearance of permanent plastic strains close to the discontinuities.

REFERENCES

Bobaru, F. et al., 2017, “Advances in Applied Mathematics: Handbook of Peridynamic Modeling”, New York: CRC Press.

Madenci, E., Oterkus, E., 2014, “Peridynamic Theory and Its Applications”, Springer: New York, USA.

Madenci, E., Oterkus, S., 2016 “Ordinary State-based Peridynamics for Plastic Deformation According to Von Mises Yield Criteria with Isotropic Hardening”, Aerospace and Mechanical Engineering, Vol. 86, pp. 192-219.

Oakley, D. R., Knight., N. F., Jr., 1995, “Adaptive Dynamic Relaxation Algorithm for Non-linear Hyperelastic Structures – Part I. Formulation”, Computer Methods in Applied Mechanics and Engineering, Vol.126, pp. 67-89.

Sarego, G. et al., 2016, “Linearized State-based Peridynamics for 2-D Problems”, International Journal for Numerical Methods in Engineering, Vol.108, pp. 1174-1197.

Villani, A. P. G. et al., 2015, “The Postbuckling Behavior of Adhesively Bonded Stiffened Panels Subject to In-plane Shear Loading”, Aerospace Science and Technology, Vol.46, pp. 30-41.

RESPONSIBILITY NOTICE

The author(s) is (are) the only responsible for the printed material included in this paper.